SANDIA REPORT
SAND2001-0757
Unlimited Release
Printed March 2001

Active Control of Magnetically Levitated Bearings

Patrick S. Barney, James P. Lauffer, James M. Redmond, William N. Sullivan

Prepared by
Sandia National Laboratories
Albuquerque, New Mexico 87185 and Livermore, California 94550

Sandia is a multiprogram laboratory operated by Sandia Corporation, a Lockheed Martin Company, for the United States Department of Energy under Contract DE-AC04-94AL85000.

Issued by Sandia National Laboratories, operated for the United States Department of Energy by Sandia Corporation.

Available to DOE and DOE contractors from
U.S. Department of Energy
Office of Scientific and Technical Information
P.O. Box 62
Oak Ridge, TN 37831

Telephone: (865)576-8401
Facsimile: (865)576-5728
E-Mail: reports@adonis.osti.gov
Online ordering: http://www.doe.gov/bridge

Available to the public from
U.S. Department of Commerce
National Technical Information Service
5285 Port Royal Rd
Springfield, VA 22161

Telephone: (800)553-6847
Facsimile: (703)605-6900
E-Mail: orders@ntis.fedworld.gov
Online order: http://www.ntis.gov/ordering.htm

SAND2001-0757
Unlimited Release
Printed March 2001

Active Control of Magnetically Levitated Bearings

Patrick S. Barney
Control Subsystems Department

James P. Lauffer
Engineering Mechanics Modeling and Simulation

James M. Redmond
Structural Dynamic Development and Smart Structures

William N. Sullivan
Manufacturing Science and Technology

Sandia National Laboratories
PO Box 5800
Albuquerque, NM 87185-0501

Abstract

This report summarizes experimental and test results from a two year LDRD project entitled **Real Time Error Correction Using Electromagnetic Bearing Spindles.** This project was designed to explore various control schemes for levitating magnetic bearings with the goal of obtaining high precision location of the spindle and exceptionally high rotational speeds. As part of this work, several adaptive control schemes were devised, analyzed, and implemented on an experimental magnetic bearing system. Measured results, which indicated precision positional control of the spindle was possible, agreed reasonably well with simulations. Testing also indicated that the magnetic bearing systems were capable of very high rotational speeds but were still not immune to traditional structural dynamic limitations caused by spindle flexibility effects.

There were three separate papers written on various advanced schemes for levitating the bearing. Two of these papers presented at the International Modal Analysis Conference (IMAC) in February 2000, and the ASME International Mechanical Engineering Congress and Exposition in November 2000) are included in this report as appendices.

Acknowledgements

The authors would like to thank Brad Paden (Magnetic Moments, Inc) who shared much of his valuable experience with magnetic bearing systems and developed the MBC 500 that was used extensively in this project. Professor Gordon Parker and his student Rebecca Petteys of Michigan Technical University contributed significantly to the theoretical and experimental work presented in this report.

Introduction and Results

Supporting rotating spindles with magnetic bearings offers a number of advantages over conventional fluid or ball/roller bearings. Magnetic bearings generally have very low drag, do not require any lubrication, and there is no physical contact between the spindle and the bearing. These characteristics make these bearings very useful for applications where low friction, high speed, cleanliness, and maintenance free life are needed. A number of systems (precision gyroscopes and artificial heart pumps are examples) have been built utilizing these advantages.

Magnetic bearings have some disadvantages as well. They are usually unstable and require active control systems to ensure the spindle is properly levitated within the journal. Their stiffness is relatively low, compared to conventional bearings. They are more expensive and bulkier than conventional bearings, mainly due to the size of magnets needed and the supporting equipment required.

This LDRD project started out with the goal of looking at improved control algorithms that could levitate a magnetic bearing more precisely and adjust for changing load conditions on the spindle. This sort of control was envisioned as enabling magnetic bearings to be more suitable for high speed or micro machining applications, where high RPM and very precise control of the spindle location are necessary. To evaluate alternative control schemes and explore the high RPM capabilities, a laboratory scale magnetic bearing demonstrator (MBC 500) was procured from Magnetic Moments, Inc. This system came with its own internal controls that levitated the bearing. In addition, the setup allowed insertion of alternative controllers either in parallel or in replacement of the built-in controller. This proved to be a very useful setup for evaluating a variety of control algorithms. Several modifications were made to the spindle and its air turbine drive to explore the high RPM performance envelope.

Two adaptive control schemes were implemented and evaluated. The first, an adaptive LMS (Least Mean Squares) controller was created with a programmable digital signal processing (DSP) card and installed in parallel to the built-in controller. This controller was able to effectively center a wobble in the system due to shaft imbalance. The results of this work are summarized in Appendix A. The second controller used an APACA (Amplitude-Phase Adaptive Control Algorithm) approach. This controller was implemented similarly to the LMS algorithm, and the results summarized Appendix B.

Both adaptive algorithms were mathematically modeled using a commercial, general purpose simulation tool (Simulink®) and the results were compared with measurements on the MBC 500 demonstrator. The agreement between test and experiment was quite good, and both adaptive controllers offered significant improvement in spindle concentricity in the bearing relative to the built-in, non-adaptive controller.

A limited number of tests were conducted with the LMS algorithm to determine the maximum speed capability of the MBC 500 bearing demonstrator. The first series of tests showed that the LMS algorithm adapted well to reduce eccentricity due to

imbalance, but the algorithm was still incapable of stabilizing the shaft through its first critical frequency at 40,000 RPM. Although efforts were made to balance the shaft more precisely and to modify the drive turbine to accelerate the shaft more rapidly through the first critical speed, this still did not allow speeds above 40,000 RPM.

Magnetic Moments eventually modified our MBC 500 with a much shorter shaft that would have a correspondingly higher first bending mode and critical speed. Maximum RPM with this system operating with the LMS algorithm was approximately 120,000 RPM.

Conclusions

The experiments and analysis of controllers indicate that magnetic bearing systems are well suited for control using modern automatic control algorithms. The adaptive algorithms investigated are capable of producing stable bearing performance while reducing eccentricity errors due to applied loads. They are relatively easy to implement with today's programmable digital signal processing capabilities.

Magnetic bearings are indeed capable of very high rotational speeds, and we successfully drove our spindle to 120,000 RPM. However, the controllability of the bearing did not allow the spindle to overcome traditional structural dynamic limitations on spindle speeds caused by vibrational modes in the spindle.

APPENDIX A

Active Control of a Magnetically Levitated Spindle

Partick Barney, James Lauffer, James Redmond, William Sullivan
Sandia National Laboratories.

Presented at the International Modal Analysis Conference
February 2000
San Antonio, TX

ACTIVE CONTROL OF A MAGNETICALLY LEVITATED SPINDLE *

Patrick Barney[1] , James Lauffer[1], James Redmond[2], William Sullivan[3]

Sandia National Laboratories
Albuquerque, NM 87185
[1]Experimental Structural Dynamics Department MS 0557
[2]Structural Dynamics and Vibration Control Department MS 0847
[3]Mechanical Engineering Department MS 0958

ABSTRACT

Active magnetic bearing (AMB) technology has received significant attention especially in applications where contaminants are an issue. AMBs offer some important advantages over conventional ball, roller or journal bearings such as no physical contact in the bearing and consequently, no need for lubricants. Additionally, given the active actuator capabilities, the AMB is well suited to controlling shaft position and therefore offers the potential for actively balancing spindles and micro-shaping capabilities for machine tools.

This work focuses on utilizing AMB actuator capabilities to dynamically center spindles. In this study, an intentionally unbalanced spindle was actively centered using an AMB. To perform this task, a modeling, simulation and test program was implemented to design the adaptive Least Mean Square (LMS) controller. The LMS controller was implemented on the MBC500 where significantly improved the concentricity of the unbalanced shaft. This paper presents the dynamic system analysis, model validation, control simulation and implementation of the multi-axis spindle centering AMB project.

INTRODUCTION

An active magnetic bearing typically consists of three or more electromagnets, each of which exerts an attractive force on the ferromagnetic rotor, levitating it without contact. These bearing systems are inherently unstable and control systems are needed to levitate and control the shaft within the magnetic journal. Commercial applications of the AMB are currently limited to high cost or high consequence applications that primarily take advantage of the lack of particulate contamination inherent to the AMB. These applications include a left-ventricular assist device (an artificial heart) and vacuum pumps.

This project investigated some of the issues of using AMBs in a machine tool environment. Specifically, the issue of shaft imbalance was addressed for high-peed spindles used in machining applications. There are several advantages of high-speed machining such as reduced cutting forces, lower heating rates, and minimal coolant consumption as compared to conventional machining processes. The high-bandwidth error-correction capability of AMBs can minimize dimensional errors while producing superior surface finishes. AMB systems also offer very high-speed capabilities without encountering the wear and lubrication problems seen by conventional bearings. The disadvantages are the additional cost and reduced static stiffness of the bearing compared to conventional bearings.

This study involves the implementation of an LMS digital control algorithm to maintain concentricity of an intentionally unbalanced spindle. A system model was constructed and, where possible, the system subcomponents were modeled and validated. The model was used in a simulation environment to predict the performance of the LMS algorithm. It was determined that the system was decoupled so that the three dimensional system could be modeled as two separate two-dimensional systems. The LMS controller was implemented on an AMB system using a programmable digital signal processor (DSP). Testing of the controlled system at 12,000 rpm indicated that the LMS control provided excellent shaft concentricity which agreed well with the simulation.

EXPERIMENTAL TESTBED

The bearing system used for this study was the MBC500 from Magnetic Moments, Inc. The MBC500 consists of two sets of active magnetic bearings supporting a simple spindle. The spindle is actively positioned in the radial direction using the

* Sandia National Laboratories is a multiprogram laboratory operated by Sandia Corporation, a Lockheed Martin Company, for the United States Department of Energy under Contract DE-AC04-94AL85000.

integrated analog sensor and control system. The shaft rotates about its longitudinal axis and is driven by an air turbine to speeds above 40,000 RPM. To provide a completely self-contained system, the controllers, sensors, actuators and conditioners were all integrated into the MBC500[1]. The system accommodated teeing into the sensors and actuators as well as bypassing the internal controllers which made the MBC500 an excellent choice for AMB control design.

SIMULATION MODEL

The AMB system was modeled using a general purpose simulation environment (Simulink®). The need for a time-marching non-linear simulation environment was due to the non-linearities in the electromagnets and sensors. The purpose of the simulation was to aid in predicting the performance of the LMS. The system block diagram model of the MBC500 is shown in Figure 1.

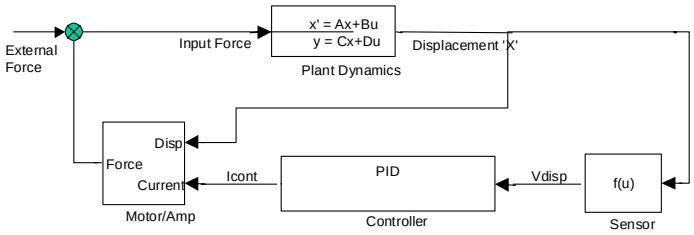

Figure 1 – System block diagram

As seen in the block diagram the major system components include the plant (the simple spindle dynamics), the sensor (eddy current), the internal analog controller (Proportional-Integral-Derivative) and the actuator (AMB). The following sections describe the modeling of each of the system subcomponents.

Plant Dynamics

In the system model shown in Figure 1, plant dynamics consist of the free-free modes of the shaft. Since the gyroscopic affects are negligible, and the system is symmetric (mechanically and electrically), the model was reduced to a two-dimensional system. Although the system never goes through a critical speed for these tests, it is important to model the spindle flexible-body dynamics to obtain good control simulation fidelity. In this case, the first bending modes of the two dimensional shaft were included in this simulation. A simple Finite Element Analysis (FEA) was performed using free-free conditions to obtain the dynamic equations. The first two bending modes for the spindle are shown in Figure 3 along with the AMB force input locations.

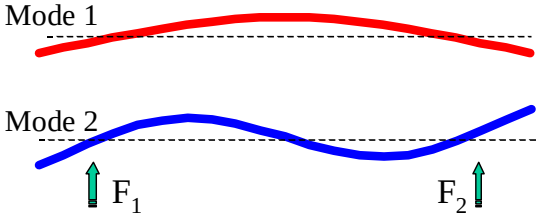

Figure 2 – First two bending modes of the spindle.

The analytically derived mass and stiffness matrices were augmented with an experimentally derived damping matrix. Using the rigid-body and flexible-body equations the plant state-space model was assembled as shown in Equation 1 below.

$$\begin{aligned} \dot{X}_P &= A_P X_P + B_P F_P \\ Y_P &= C_P X_P \end{aligned} \qquad (1)$$

where 'P' signifies the plant matrices and states. In this model, the restoring forces of the plant (shaft) are those exerted by the magnets, which are not included in the state-space model. These AMB forces are used as the inputs (F) to the state-space model, while the outputs (Y) of the system are the positions of the shaft.

Sensor Dynamics

The control feedback sensors for this AMB system consist of two orthogonal eddy current proximity probes at each shaft end near the AMB center of force (nearly colocated). The target for the eddy current sensors is the circular shaft that inherently makes the output of voltage versus displacement somewhat non-linear in the operating region. The output voltage with respect to meters displacement is given as

$$V_{sense_i} = 5000 X_i + 24 \times 10^9 X_i^{\,3} \qquad (2)$$

Figure 3 provides the displacement versus voltage for a given axis. As can be seen by the plot, the output is relatively linear for small deflections but the non-linearity becomes more pronounced at the higher displacement levels (hardening spring effect). The range of motion for the MBC500 shaft is .0004 meters; Figure 3 is shown with a range to .0003 meters to de-emphasize the stronger non-linear affects with displacements above .0003 meters.

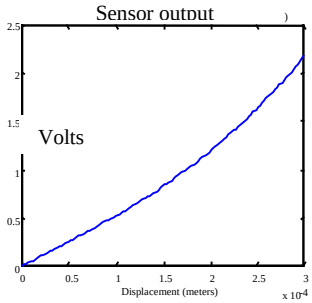

Figure 3 – Eddy current sensor voltage output vs. displacement

Controller Dynamics

There are four independent PID analog controllers supplied with the MBC500. Each controller uses a single axis sensor voltage as input and produces an output voltage that controls the

magnetic force (a pair of pull-pull magnets) for that particular axis. The transfer function for the controller is

$$V_{control} = \left(\frac{1.41(1+8.9\times10^{-4}s)}{(1+3.3\times10^{-4}s)(1+2.2\times10^{-5}s)} \right) V_{sense} \quad (3)$$

The implementation is primarily proportional feedback of the sensor displacement. For a truly colocated sensor-actuator pair and a linear uncoupled system, this is a very robust controller, and for this application it works very well. In essence, the proportional displacement feedback offers a virtual stiffness to the system that results in a bounce mode at about 70 hertz and a pitch mode at about 45 hertz. The non-linearity in the system (mostly due to the actuator) adds effective damping to the system and the result is a well behaved mechanical system.

Active Magnetic Motor Dynamics

The magnets can only exert an attractive force so each bearing consists of four electromagnets. These electromagnets are positioned in a simple opposing pull-pull arrangement for each orthogonal axis at each end of the spindle. A simple cartoon diagram of a single electromagnet is shown in Figure 4.

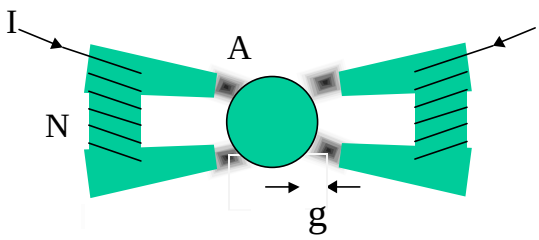

Figure 4 – Simple electromagnet, ferous target and resultant forces.

The force exerted by one electromagnet on the shaft is

$$F = \frac{A\mu_0 N^2 I^2}{4g^2} \quad (4)$$

where A is the cross-sectional area of the magnet, μ0 is the permittivity of free space, g is the gap between the electromagnet and the rotor, and N is the number of coils in the magnet, each carrying current I. The MBC500 has a gap of 0.0004 meters and a bias current of 0.5 amperes at equilibrium. The total force on the shaft at one bearing due to both magnets (in one axis) is

$$F = k\frac{(I-0.5)^2}{(x+0.0004)^2} - k\frac{(I+0.5)^2}{(x-0.0004)^2} \quad (5)$$

where k = Aμ0N2/4.

As can be seen by the equation above, the output force of the AMB is highly non-linear with respect to the inputs; the force is proportional to the square of the controller current, and is inversely proportional to the square of the gap. Figure 5 provides an output force map from the actuator as a function of control voltage and shaft displacement. As can be seen by this figure, the output forces become highly non-linear as both the displacement and control voltage become large.

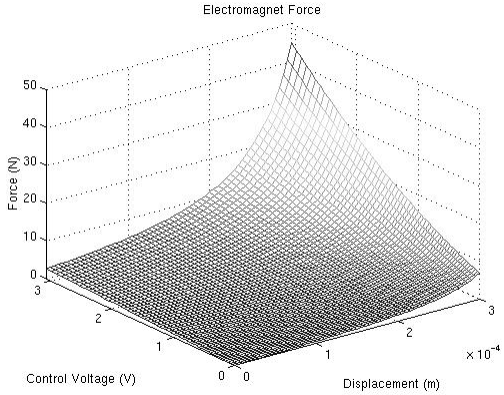

Figure 5 – AMB force output as a function of bearing gap and control voltage.

Modeling the closed loop system

As discussed earlier, a full simulation of the AMB system is necessary because of the non-linearities in the system. Strong system non-linearities do not allow for accurate linear analysis when trying to predict the response of a system especially when it is to be used for closed-loop control-algorithm development. Because of this, a time marching simulation method must be employed to offer reasonable prediction accuracy. Additionally, the operating amplitudes of the simulation must be close to those expected in service (or in the validation experiments) or the resulting predictions may have significant errors. The basic model was first exercised using Simulink® to produce model validation data as presented in the following sections. Next, the model was used to determine the effectiveness of an LMS algorithm for mitigating shaft eccentricity.

System Validation

The validation of a system model for predictive simulation typically requires a great effort. The first step in the process is to determine how success will be qualified in terms of the goal of the prediction and the significance of the error sources. In this case, the purpose of the simulation was to evaluate alternative control approaches to the imbalance problem of an AMB shaft. Particularly, the LMS algorithm was being evaluated for its performance in a steady state mode of operation.

To perform this task, it was assumed that a good representation of the rigid-body modes of the system was important. The representation selected for this comparison task was the system FRF from AMB actuator forces to the sensor deflections near a nominal operating amplitude. Figure 6 provides the simulated and measured FRFs for input at one actuator and its respective response. As can be seen, the model compares well at the resonance. The deviation of the FRF off resonance (especially at the low frequencies) will not particularly affect the

response of the LMS imbalance at the selected 200 hertz (12,000 RPM) operating point.

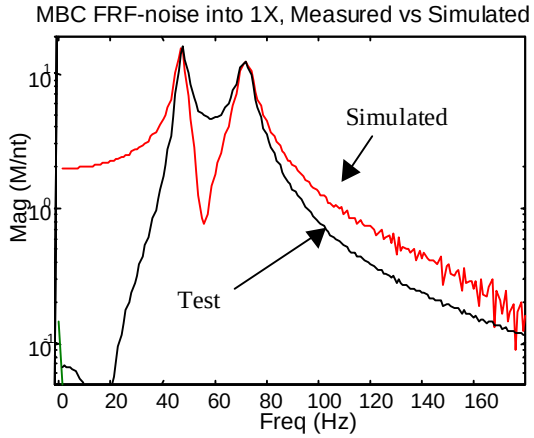

Figure 6 – Measured FRF versus simulated.

In addition to the rigid-body and control dynamics, the flexible-body dynamics of the shaft are usually of importance. Although this simulation operates at frequencies well below the lowest flexible-body mode, the lowest two were included in the model for completeness. These flexible-body dynamics were validated with test. Figure 7 provides the measured and simulated driving-point FRFs for one axis. As can be seen, these functions agree quite well in the regions near the system flexible-body modes.

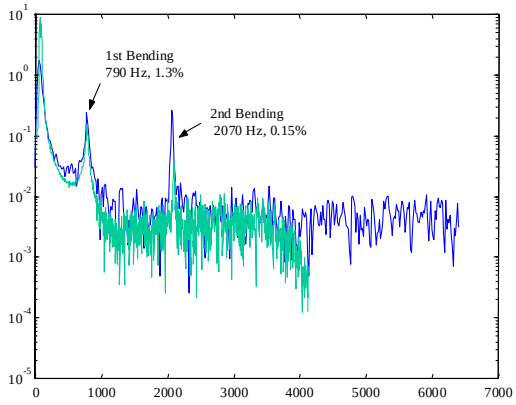

Figure 7 –Simulated versus measured FRF for flexible-body modes.

LMS Adaptive Control

The LMS adaptive control strategy is a technique that has received considerable attention over the last 20 years[2-5]; however, it was the advent of the digital signal processor (DSP) and lower cost system components that has inspired its popularity today. In its primitive state, the LMS algorithm is a gradient descent algorithm used for system identification whose result is used in an FIR implementation to produce a cancellation signal. The cancellation signal is then added to the primary signal (usually mechanically) to produce the resultant error signal which is ideally much smaller than the original primary signal. The modern uses of LMS for active noise cancellation have shown excellent performance for applications such as interior cabin noise cancellation for propeller driven aircraft.

The basic idea of LMS control is shown in Figure 8. As can be seen in this simple diagram, there is a reference signal that is convolved with a time varying weighting function which produces the output signal (y) which is added to the primary signal (p) to produce the error signal (e).

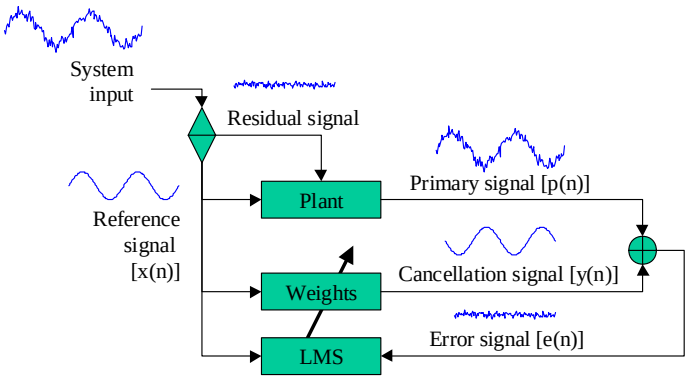

Figure 8 – Functional diagram of the LMS algorithm

The equation below describes the FIR convolution of the current filter weights (w) by the reference signal (x),

$$y(n) = \sum_{i=0}^{N-1} w_i(n) \cdot x(n-i) \qquad (6)$$

where N is referred to as the number of taps.

The kernel of the gradient descent algorithm used to update the weights in the LMS implementation is described in the following equation. As shown, the weights (w) are updated by the current error value (e), the reference vector (x) and a user specified scalar (μ),

$$w_i(n+1) = w_i(n) - \mu \cdot e(n) \cdot x(n-i), i = 0 \ldots N-1 \qquad (7)$$

The cancellation signal is added to the primary noise signal to produce a resultant error signal which ideally is significantly smaller that the original primary signal. The LMS algorithm is a feed-forward controller (usually inherently stable) but the rapid updating of the weighting function could result in an unstable control. The user's choice of μ, error scaling factors, number of taps (length of the weighting filter) and sample rate all play a significant role in the stability of the implementation.

Application of LMS to AMB

Although the LMS was once seen as a cure all, its commercial implementations have been limited to a few active noise cancellation products. The reason for the lack of customer acceptance appears to be threefold: 1) cost of implementation compared to the alternative passive methods, 2) poor performance due to inappropriate applications and 3) potential for instability. Of the three reasons listed, the inappropriate use of the LMS has been the most significant contributor. Like many new technologies developed for particular applications there is a desire to apply the technique to a much wider field. The practical implementation of the LMS algorithm is particularly well suited for low frequency (below 300 hertz) periodic signals. Ideally, the signal to be controlled would be constructed of one or two primary frequencies with some possible broadband noise. Any potential LMS application should be tested for this at the preliminary stages, followed by examination of the practical aspects.

In the case of the AMB and shaft imbalance, the LMS implementation is a very good fit. Given the nominal operating speed of 12,000 RPM (200 hertz) and a simple imbalance (stationary single sinusoidal) the system meets the primary requirement of low frequency and a few tones. The fact that sensors and actuators already exist for any AMB system makes the implementation very practical. The shaft imbalance problem has an additional advantage in the fact that the system axes are uncoupled so that simple single-input/single-output (SISO) algorithms can be employed reducing the performance requirements for the DSP.

In essence, the run-out of the shaft is picked up by the displacement sensor in the AMB bearing, this signal becomes the error signal (primary signal) to be minimized. Given that the signal can be minimized, then the shaft would become more geometrically centered with respect to the bearing housing.

LMS Simulation

The basic time domain LMS algorithm was implemented in both simulation and experiment. The LMS system model utilized the validated Simulink® model as a basis with the addition of a imbalance forcing function and an LMS feedforward algorithm. The figure below provides the block diagram for the LMS system model.

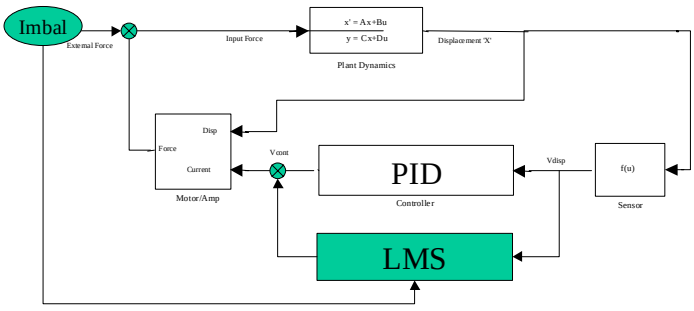

Figure 9 – Block diagram of AMB controller with LMS algorithm and imbalance excitation force.

As can be seen in the figure, there is the basic PID inner loop with the additional LMS control loop wrapped around it. In the case of the simulation, the standard SISO digital implementation of the LMS was implemented. In this particular case, the bearing 1 X axis was chosen, although the simulation predicted the responses in all axes.

The required inputs to the LMS algorithm are the reference signal and the error signal. In this simulation, a sinusoidal forcing function was generated at a frequency (200 hertz) and amplitude consistent with the test configuration. The forcing function simulated a mass imbalance at the bearing 1 X and Y axes. This forcing function was also used as the LMS reference signal because it was coherent with the error signal to be attenuated. In practice, the equivalent quality signal is derived from the tachometer. The error signal was the simulated voltage from the eddy current sensor located at 1 X. The resultant LMS output signal was added to the control voltage and injected to the AMB.

The LMS parameters investigated during the control algorithm development included the effective sample rate of the analog-to-digital (A/D) converter, the number of taps of the weighting vector and the convergence coefficient (μ).

Figure 10 provides a summary of the results of the simulation. Again, the imbalance was simulated at one end of the shaft in both directions. The upper plot is the X displacement versus time, while the lower plot is the Y displacement versus time. At the start of the simulation, both axes have equal sinusoidal runnout (.000075 meters) due to the imbalance. As seen by the X displacement (the control axis), the LMS control quickly moves towards reduction of the error signal. At the end of the three second simulation, the error signal is attenuated by a factor of ten. The cross axis coupling (to the Y axis) is near zero as seen by the fact that the uncontrolled Y axis is not affected by the control forces injected at the X axis.

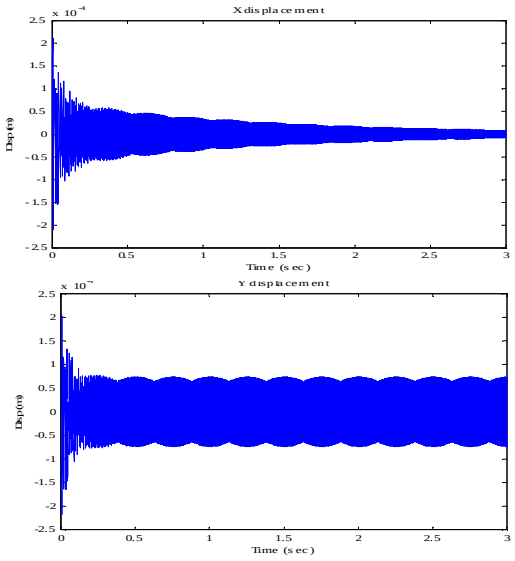

Figure 10 – Simulated system response for LMS control convergence.

LMS Experiment

The basic time domain LMS algorithm was implemented in experiment using the MBC500 and the LMS simulation approach. The natural imbalance of the shaft was sufficient for reasonable eccentric rotation at 12,000 RPM. The once per revolution tachometer provided a very clean signal which was coherent with the imbalance as required for LMS.

The PC-based DSP system was programmed for a SISO LMS with the capability to update μ in real-time. The nominal parameters from simulation were used in the baseline DSP implementation and are given in Table 1

Table 1 – DSP parameters determined from simulation.

sample frequency	2000 Hz
Filter length (w)	20 taps
μ	Variable
Reference	Tachometer

As shown in the table, μ was selected as variable to account for scaling issues within the A/D of the DSP.

Figure 11 provides a summary of the results of the test. The upper plot is the X displacement (volts) versus time, while the lower plot is the Y displacement (volts) versus time. At the start of the simulation, both axes have equal sinusoidal run-out (.000075 meters) due to the imbalance. As seen by the X displacement (the control axis), the LMS control quickly attenuates the error signal (orders of magnitude). The cross axis coupling (to the Y axis) is near zero as seen by the fact that the uncontrolled Y axis is not affected by the control forces injected at the X axis.

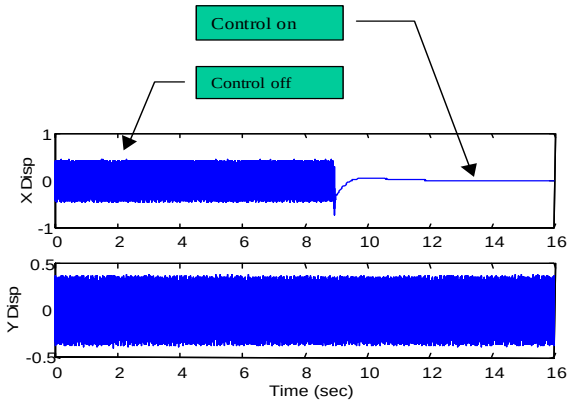

Figure 11 –LMS implementation on AMB shaft imbalance (control on versus control off).

Compared to the simulation, the results of this test are very good and converge even more quickly. The reason for the quicker convergence is that the μ used in the test was higher than that of the simulation. Although the attenuation of the imbalance is fast, the impulsive nature of the control force when first activated causes a rigid-body motion which takes a few seconds to settle out.

Multi-Axis Experiment

As stated earlier, it was suspected and confirmed through modal experiments that the system axes were reasonably decoupled. Due to the uncoupled system dynamics, the single axis LMS control experiment could be extended to two independent control implementations. The single tachometer signal and the displacement error signals were fed into separate LMS algorithms which produced independent control signals. Figure 12 presents the measured shaft deflections for the two-axis LMS control off versus LMS on.

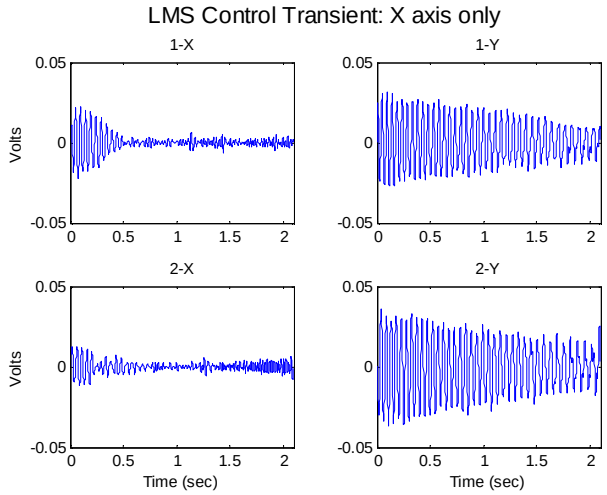

Figure 12 – Measured shaft deflections for the two-axis LMS control.

As can be seen in the figure, at the start there is a significant once per revolution displacement on all axes due to the imbalance. At 0.3 seconds, the control is turned on for the X axes and their displacements are significantly reduced. The Y axes deflections are also somewhat reduced over time.
Figure 13 provides similar results for the four axes LMS implementation. As can be seen by the plot, all axis have significant reduction of the out-of-roundness errors.

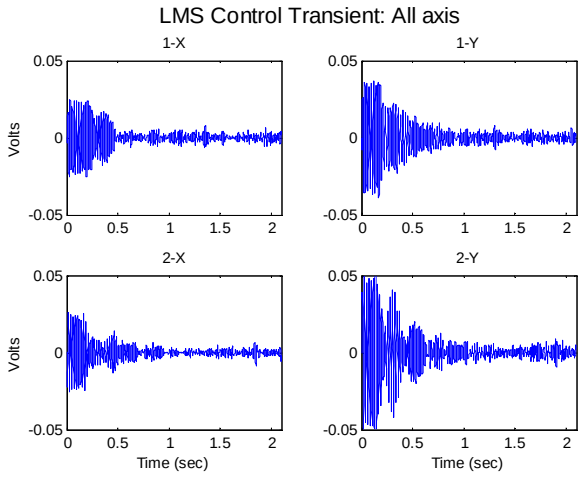

Figure 13 – Measured shaft deflections for the four-axis LMS control.

Figure 14 provides a typical displacement PSD for a signal axis with and without control. The dominant peak seen in the figure is the once per revolution eccentricity of the shaft without LMS control. The lack of that peak for the LMS control "on" case shows the effectiveness of the controller.

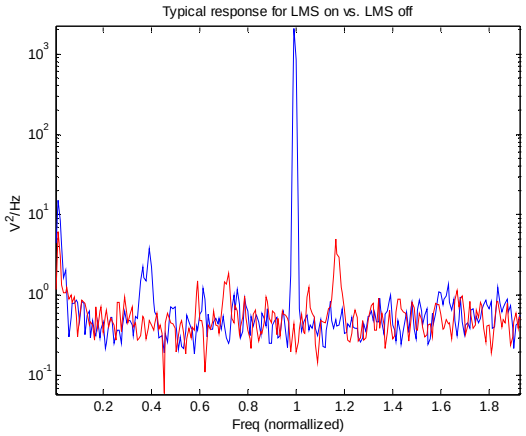

Figure 14 – Typical PSD of measured displacement with and without LMS control.

It should be noted that the LMS controller can only produce energy at the frequencies contained in the reference signal. In this case that means that only the once per revolution frequency could be produced from the LMS control and subsequently injected into the MBC500. Although a single frequency may be injected into the MBC, the non-linear nature of the AMB could produce strong harmonics which would not be controlled by the LMS. This coupled with a small DC bias in the DSP would at times increase the RMS deflections of the shaft, although for most measurements this was not an issue.

Application to Critical Speed

The natural question of the AMB/LMS control philosophy is its ability to go through system critical speeds. Typically there are three methods used for getting through a system critical speed: shaft balancing, high slew rates and adding damping. The next few paragraphs discuss the possibilities of using the AMB to implement these techniques.

Although it may seem that the spindle centering translates into a balanced shaft, this is not true. In fact, geometric centering may actually create more imbalance forces in the system which would worsen the issue of critical speed excitation. Since a general system may require multiplane balancing, it is unlikely that the AMB system would be able to contribute to going through the critical by active centering.

There have been many active control applications which have added damping to a system. To efficiently use active control to increase system damping, the actuator must be placed at a location which are well matched to the modes to control[6]. A good measure of the effectiveness of an actuator to a given mode is the normalized length of the input shape vector. It is apparent from the mode shapes in Figure 2 that the locations of the AMB forces are not optimal for contributing to those modes. In fact, the AMB excitation locations are close to the nodal points for both modes; although they are quite good for the rigid-body modes for which they were intended. Table 2 provides the norm of the input shape vectors for modes one and two given the AMB actuator force locations. As can be seen by the table, the norms are very low (compared to a value of 1.0) which indicates that these are poor locations for controlling the modes. Without a good coupling of the actuator forces to the mode, the ability to perform active damping is poor and it is suspected that this is the case for AMB modal damping.

Table 2 – Controllability of modes 1 and 2 given the AMB locations

Mode number	Norm of input vector
1	0.056
2	0.227

Another method of getting through critical speeds is to use a high slew rate (fast rate of change of the RPM). This effectively reduces the excitation energy going into the particular mode by reducing the time spent at that modal frequency. Although the AMB control cannot contribute to the slew rate, it may be able to change the modal frequency. By changing the modal frequency from a high value to a lower value over a short period of time, an effective high slew rate could be achieved. Unfortunately the placement of the actuators result in low controllability and therefore this approach may not be feasible with the current AMB configuration.

Conclusions

The work presented in this paper concentrated on an AMB test program that utilized the actuator capability to dynamically center a spindle. An unbalanced AMB spindle system was enhanced with an LMS (Least Mean Squares) algorithm wrapped over an existing PID rigid-body controller. The enhanced controller improved the concentricity of the MBC500 imbalanced shaft by two orders of magnitude.

The methods and the implementation of predictive simulation, model validation and test implementation were shown here to be useful for control development. Additional efforts will be pursued which address high slew rate operations and alternative error signals. The LMS control approach of AMB systems presented in this paper are extendable to reduction of forces into the bearing housing (a notch filter) and possibly force minimization through critical speed resonance.

ACKNOWLEDGMENTS

The authors wish to thank Professor Brad Paden of the University of California at Santa Barbara and Magnetic Moments, Inc. and Professor Gordon Parker at Michigan Technological University for their contributions to this project.

REFERENCES

[1] Paden, B., "Operating Manual for the MBC500", Magnetic Moments Inc., Santa Barbara CA.

[2] Lueg, P., June 1936 "Process of Silencing Sound Oscillations," U.S. Patent No. 2,043,416.

[3] Widrow, B., and S. D. Stearns, 1985, "Adaptive Signal Processing", Prentice-Hall, Englewood Cliffs, NJ.

[4] Elliott, S. J., P. A. Nelson, I. M. Stothers and C. C. Boucher, 1990, “In-Flight Experiments on the Active Control of Propeller-Induced Cabin Noise”, Journal of Sound and Vibration, Vol. 140, No. 2. pp. 219–238.

[5] Kuo, S. M., and C. Chen, 1990, “Implementation of Adaptive Filters with the TMS320C25 or the TMS320C30,” Digital Signal Processing Applications with the TMS320 Family, Volume 3, edited by P. Papamichalis, Prentice-Hall, Englewood Cliffs, NJ, pp. 191–271.

[6] J. Redmond, P. Barney, and D. Smith, January 1999, "A Biaxial Actively Damped Boring Bar For Chatter Mitigation" International Journal of Manufacturing Science and Production”, Vol. 2, No. 1, pp 1-16.

APPENDIX B

Disturbance Rejection Control of an Electromagnetic Bearing Spindle

Rebecca Petteys and Gordon Parker
Michigan Technological University

James Redmond
Sandia National Laboratories.

Presented at the ASME International Mechanical Engineering Congress and Exposition
November 2000
Orlando, FL
"Adaptive Structures and Material Systems," AD-Vol. 60, pp. 461-468.

Disturbance Rejection Control of an Electromagnetic Bearing Spindle

Rebecca Petteys
Gordon Parker
Michigan Technological University
Department of Mechanical Engineering
1400 Townsend Dr.
Houghton, MI 49931

James Redmond
Sandia National Laboratories
Albuquerque, NM 87111

ASTRACT

The force exerted on the rotor by an active magnetic bearing is determined by the current flow in the magnet coils. This force can be controlled very precisely, making magnetic bearings a potential benefit for grinding, where cutting forces act as external disturbances on the shaft, resulting in degraded part finish. It is possible to achieve precise shaft positioning, reduce vibration of the shaft caused by external disturbances, and even damp out resonant modes. Adaptive control is an appealing approach for these systems because the controller can tune itself to account for an unknown periodic disturbance, such as cutting or grinding forces, injected in to the system. In this paper we show how one adaptive control algorithm can be applied to an AMB system with a periodic disturbance applied to the rotor. An adaptive algorithm was developed and implemented in both simulation and hardware, yielding significant reductions in rotor displacement in the presence of an external excitation. Ultimately, this type of algorithm could be applied to a magnetic bearing grinder to reduce unwanted motion of the spindle which leads to poor part finish and chatter.

INTRODUCTION

In magnetic bearing systems, a spindle is levitated with magnetic fields created by either permanent magnets or electromagnets (or both) so that no part of the spindle comes in contact with the bearings. With permanent magnets, the force exerted on the rotor can be either attractive or repulsive. A repulsive force results in a system that is stable without a controller. However, the force exerted by the permanent magnets cannot be controlled and is limited by the strength of the magnets. With electromagnets, the force on the rotor can be varied by changing the current flow in the magnet coils. This results in an active magnetic bearing (AMB). However, the levitating forces are attractive, making the system inherently unstable and requiring the use of a controller.

The force exerted by the electromagnets can be controlled within ± 0.05 N, making it possible to achieve precise shaft positioning, reduce vibration of the shaft caused by external disturbances, and even damp out resonant modes. This makes magnetic bearings a potential benefit for grinding and other

metal cutting processes, where cutting forces act as external disturbances on the shaft, resulting in degraded part finish. AMB systems also do not have the wear and lubrication problems seen by conventional bearings, but require additional electronic and cooling systems. Furthermore, they are limited in load capability

Adaptive control is an appealing approach for these systems because the controller can tune itself to account for an unknown periodic disturbance, such as cutting forces injected in to the system. In this paper we show how one adaptive control algorithm can be applied to an AMB system with a periodic disturbance applied to the rotor. The purpose is to create an input signal that would counteract the disturbance and result in minimal motion of the spindle. In an application such as grinding, this would result in improved part finish, reduction of chatter, etc. First a model of the experimental system must be developed to test the proposed control strategy. Then the adaptive control algorithm will be described and results will be shown.

EXPERIMENTAL SETUP

The bearing system modelled and used for this paper is a modified MBC500 from Magnetic Moments, Inc. The MBC500 has two active magnetic bearings, each consisting of four electromagnets, supporting the spindle. The bearings are mounted on top of an anodized aluminum case which houses the electronics and also acts as a heat sink for the magnets. The spindle is actively positioned in the radial direction at the bearings and freely rotates about its long axis. The front panel shows a block diagram of the system with BNC connections for easy access to system inputs and outputs. An air turbine drives the shaft to speeds up to 10,000 RPM.

The system has four on-board analog lead-filter controllers that levitate the spindle in its default mode. These controllers can be disabled with switches on the front panel, allowing an external controller to be implemented. The BNC connections also allow for an external controller to be wrapped around the on-board controllers while they are still engaged. The modified version of the MBC500 include an external electromagnet mounted on the case near the center of the spindle to be used as a disturbance source. The magnet can be moved to vary the gap between the magnet and the spindle, thereby allowing for a large range of applied forces. The current flow to this magnet is controlled by an external amplifier.

SYSTEM MODEL

An accurate model of the system is necessary for designing and testing prospective control strategies. Magnetic bearings are highly nonlinear by nature and, in order to best capture the effects of those nonlinearities, a Simulink simulation was designed. A block diagram representation of the system is shown in Figure 1. This diagram represents the MBC500 without any external controllers, but with the external magnet applying a disturbance force to the spindle. It is assumed that the spindle is not spinning, so there are no gyroscopic effects and the axes are completely uncoupled. The external force is assumed to be applied exactly at the center of the shaft. The system inputs and outputs are also shown.

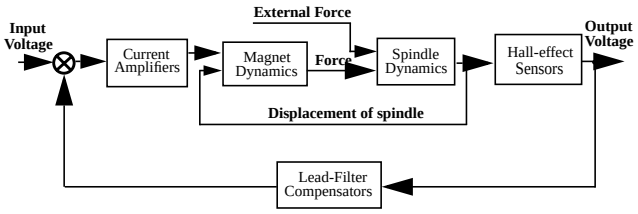

Figure 1. Simulink model used to simulate the magnetic bearing system

When external controllers are implemented, either the feedback loop containing the lead-filter compensators is broken and replaced with a computer system which implements the digital controllers, or an external controller is wrapped around the on-board compensators, leaving the feedback loop intact. For the implementation of the adaptive control algorithm presented in this paper, the on-board controllers are left intact and the external adaptive controller is wrapped around the feedback loop.

There are five main components to the system that must be included in the model: the spindle dynamics, the magnet dynamics, the on-board controllers, the current amplifiers, and the position sensors. Each is dealt with in the following sections. Definitions of the variables and parameters used in the description of the model and system are given in Table 1 and Table 2.

Table 1: Definitions of variables

x_0	displacement of center of mass of rotor
x_1 and x_2	displacement of rotor at left and right bearings
X_1 and X_2	displacement of rotor at Hall Effect sensors
θ	tilt of rotor about y-axis
F_1 and F_2	forces exerted on rotor at left and right bearings
F_e	external applied force

Table 2: Definitions of parameters

L = 0.269 m	total length of rotor

Table 2: Definitions of parameters

$l_1 = 0.024$ m	distance from each bearing to end of rotor
$l_2 = 0.0028$ m	distance from each sensor to end of rotor
$I_0 = 1.5884\times10^{-3}$ kg m^2	moment of inertia of rotor around y-axis
$m = 0.2629$ kg	mass of rotor
$a = 0.0107$ m	distance from bearing 1 to external magnet
$b = 0.0092$ m	distance from bearing 2 to external magnet

Spindle Dynamics

Both the rigid and the first two flexible body modes were incorporated into the simulation. Because the axes are uncoupled, we may look at each independently and can assume that the dynamics in each direction are the same (with the exception of the constant force of gravity in the y-direction). On the experimental set-up, the external force is applied in only the x-direction, so the equations of motion will be derived only for the x-direction.

Rigid Body Dynamics. For rigid body motion, the spindle is assumed to move without bending. (Flexible body motion will be considered in the next section.) Figure 2 shows the spindle from above. The coordinate system and variables are defined as shown.

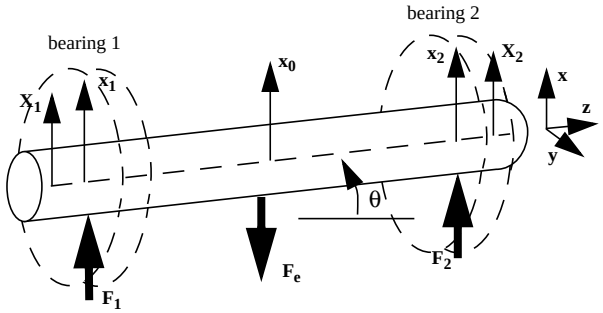

Figure 2. The spindle shown with variables defined.

The axis are uncoupled, so, assuming the spindle is radially symmetric, the x- and y-axes will have the same equations of motion (again, with the exception of the constant force of gravity in the y-direction). As shown in the figure, the sensors are located just outside the bearings along the spindle and the external force, F_e, is applied near the center of mass of the spindle in the negative x-direction.

There are two rigid body degrees of freedom for each axis. This means that there must be two independent coordinates chosen to describe the system. In this case, it is easiest to choose the position of the center of mass of the spindle, x_0, and the angle of rotation of the spindle from the equilibrium position, θ. The equations of motion for the rigid body motion in the x-direction are found by balancing the forces and moments about the center of the shaft.

$$\sum F = m\ddot{x}_0 = F_1 + F_2 - F_e \tag{1}$$

$$\sum M_0 = I_0\ddot{\theta} = (F_2 - F_1)\left(\frac{L}{2} - l_1\right) + \frac{1}{2}F_e(b-a) \tag{2}$$

The clearance at the bearings is ± 0.4 mm, so small-angle approximations are appropriate. For rigid body motion, the only restoring forces are those exerted by the magnets, which are nonlinear and cannot be included in the linear rigid body state-space model. Therefore, the state-space system is constructed such that the forces -- the external force and the bearing forces on either end of the spindle -- are the inputs and the displacements of the spindle at the bearings and sensors are the outputs. The state vector is chosen to consist of the displacement of the center of mass of the spindle, the angle of rotation and their respective time derivatives. The resulting system is shown below.

$$\dot{X_{RB}} = A_{RB}X_{RB} + B_{RB}U_{RB} \tag{3}$$

$$Y_{RB} = C_{RB}X_{RB} \tag{4}$$

where

$$X_{RB} = \begin{bmatrix} x_0 \\ \dot{x}_0 \\ \theta \\ \dot{\theta} \end{bmatrix},\ U_{RB} = \begin{bmatrix} F_1 \\ F_2 \\ F_e \end{bmatrix},\ Y_{RB} = \begin{bmatrix} X_1 \\ x_1 \\ X_2 \\ x_2 \end{bmatrix} \tag{5}$$

$$A_{RB} = \begin{bmatrix} 0 & 1 & 0 & 0 \\ 0 & 0 & 0 & 0 \\ 0 & 0 & 0 & 1 \\ 0 & 0 & 0 & 0 \end{bmatrix},\ B_{RB} = \begin{bmatrix} 0 & 0 & 0 \\ \frac{1}{m} & \frac{1}{m} & \frac{1}{m} \\ 0 & 0 & 0 \\ -\frac{1}{I_0}\left(\frac{L}{2} - l_1\right) & \frac{1}{I_0}\left(\frac{L}{2} - l_1\right) & 0 \end{bmatrix},$$

$$C_{RB} = \begin{bmatrix} 1 & 0 & -(L/2 - l_2) & 0 \\ 1 & 0 & -(L/2 - l_1) & 0 \\ 1 & 0 & (L/2 - l_2) & 0 \\ 1 & 0 & (L/2 - l_1) & 0 \end{bmatrix} \tag{6}$$

where ‘RB’ signifies the rigid body matrices and states. The output of the system depends on the sine of the tilt angle, which has been approximated as unity.

Flexible Body Dynamics. Only the first two bending modes are considered for this simulation. The mass and stiffness matrices for the shaft are taken from the MBC500 manual and are essentially the free-free modes of the shaft and damping was found experimentally to be approximately 1.3% for the first bending mode and 0.15% for the second bending mode. The modal equation for the x-direction in matrix form is then

$$M\ddot{a} + C\dot{a} + Ka = P \tag{7}$$

The state-space system for the flexible body dynamics can be developed in the same manner as the rigid body equations. They are expressed here as

$$\dot{X_{FB}} = A_{FB}X_{FB} + B_{FB}F_{FB} \tag{8}$$

$$Y_{FB} = C_{FB}X_{FB} \tag{9}$$

The inputs and outputs for this state-space system must be the same as the rigid body system, but the state vectors will be different.

The total displacement of the shaft is the combined contribution of the rigid and flexible body displacements. In other words,

$$Y_{tot} = Y_{RB} + Y_{FB} \tag{10}$$

This displacement is then the input for the position sensors.

Hall Effect Sensor Dynamics

The sensors for this system are two orthogonal Hall-effect sensors at each shaft end. The sensors are actually located closer to the ends of the shaft than the bearings (see Table 2 and Figure 2) but we will make the approximation that they are collocated. The nonlinear sensor output is

$$V_{sense_i} = 5000X_i + 24\times10^9 X_i{}^3 \tag{11}$$

for $i = 1, 2$, where X_i is measured in meters. Figure 3 shows the relationship between the sensor voltage and the displacement of the shaft. The figure also shows a plot of the above equation linearized about the equilibrium position ($X_i = 0$).

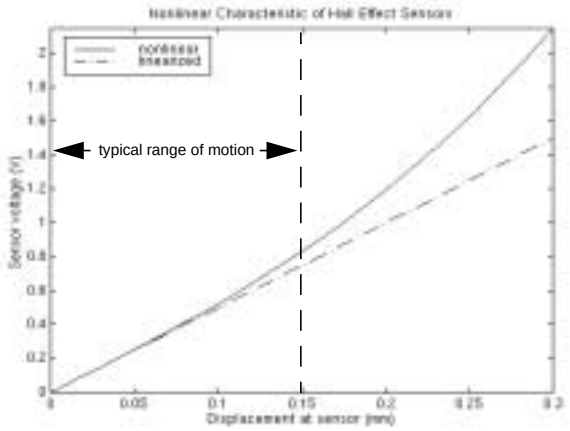

Figure 3. Graph of sensor nonlinearity

As the plot shows, the output is relatively linear for low deflections but the nonlinearity becomes more pronounced with larger displacements ($X_i > 1.5\times10^{-4}$ m). The nonlinear relation is used in the Simulink model, but, as the system usually runs with displacements less than 0.15 mm, the linearized relation could also be validly used.

Lead-Filter Compensator Dynamics

Since electromagnets can only exert an attractive force, each bearing consists of four magnets, two magnets each in the x- and y-directions. There is an analog lead-filter compensator for each of the magnet pairs. Each uses the voltage from the corresponding sensor as input and produces an output voltage. The transfer function for the compensators is

$$V_{control} = \left(\frac{1.41(1 + 8.9\times10^{-4}s)}{(1 + 3.3\times10^{-4}s)(1 + 2.2\times10^{-5}s)}\right)V_{sense} \tag{12}$$

These analog compensators can be removed from the feedback loop so that a digital controller can be implemented. However, for the purposes of this paper, the analog compensators were left in so that the adaptive controller could be implemented without exceeding the limitations of the dSpace components.

Current Amplifier Dynamics

The actuator current amplifier converts the control voltage to a current for the electromagnet according to

$$I = \frac{0.25}{1 + 2.2\times10^{-4}s}V_{control} \tag{13}$$

The amplifier, in essence, acts as a low-pass filter with a break frequency of, filtering out the very high frequency content of the input signal.

Electromagnet Dynamics

The force exerted by one electromagnet on the shaft is

$$F = \frac{A\mu_0 N^2 I^2}{4g^2} \tag{14}$$

where A is the cross-sectional area of the magnet, μ_0 is the permittivity of free space, g is the gap between the electromagnet and the rotor, and N is the number of coils in the magnet, each carrying current I. For the MBC500 at equilibrium, the gap is 0.0004 m and there is a bias current of 0.5 amps. If we define x as the displacement from equilibrium and k as $A\mu_0 N^2/4$ then the total force on the shaft at one bearing due to both magnets (in one direction) is

$$F_i = k\frac{(I_i - 0.5)^2}{(x_i + 0.0004)^2} - k\frac{(I_i + 0.5)^2}{(x_i - 0.0004)^2} \tag{15}$$

for $i = 1, 2$. Note that the force is proportional to the square of the current in the wire and is inversely proportional to the square of the gap width. This represents the strongest nonlinearity in the system. This relationship is plotted in Figure 4 for a range of displacements and currents.

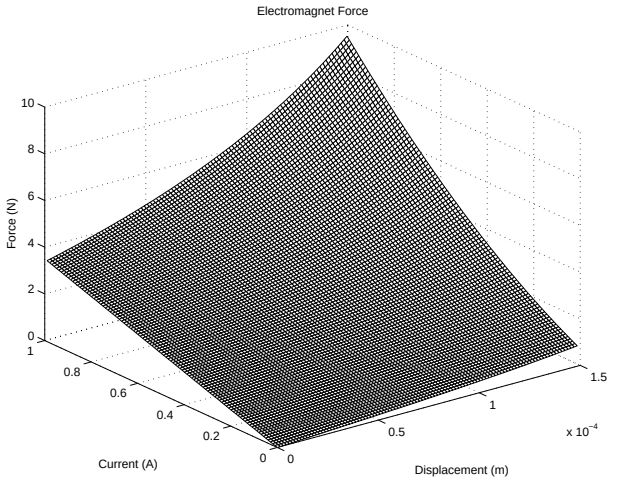

Figure 4. Graph of force exerted by the electromagnets versus current and displacement

As shown in the figure, the output forces become very non-linear and large as the displacement and control current become large. In normal operation, the displacement is rather small ($x_i < 1\times10^{-4}$ m) but the control current may still fluctuate widely because of the dynamic characteristics of the controllers.

Modeling the closed loop system

Because of the many nonlinearities in the system, a linearized state-space model was not sufficient to model the system accurately. The biggest source of nonlinearity is the magnets, since the force they exert is inversely proportional to the square of the displacement and directly proportional to the square of the control current. Near equilibrium and at steady state, this force can be approximated as linear with a spring constant of 10,500 N/m, but outside this region ($x_i > 5\times10^{-5}$ m), the approximation is invalid. Another smaller source of nonlinearity is the Hall effect sensors. A linear approximation for these is good to $X_i \approx 1.5\times10^{-4}$ m. Because of these limitations, the nonlinear model was used.

For the implementation of the adaptive control algorithm presented below, the on-board analog controllers are left in the feedback loop and the external adaptive controller is wrapped around the feedback loop.

ADAPTIVE CONTROL ALGOTRITHM

An adaptive controller called the amplitude-phase adaptive control algorithm (APACA) was designed to augment the lead-filter compensator. The purpose of APACA is to predict and compensate for the external disturbance, whereas the purpose of the lead-filter compensator is simply to levitate the spindle.

APACA is based on the MIT Rule. The MIT Rule was one of the first adaptive algorithms and is based on minimizing the cost function

$$J(\alpha) = \frac{1}{2}e^2 \tag{16}$$

where e is the error signal -- in this case, the displacement of the spindle -- and α is the parameter to be varied. This leads to the discrete equation

$$\alpha(n+1) = \alpha(n) - \gamma e(n)\frac{\partial e}{\partial \alpha} \tag{17}$$

where $\frac{\partial e}{\partial \alpha}$ is known as the sensitivity derivative.

APACA is designed to be used for external disturbances which are sinusoidal, have a known and fixed frequency, and oscillate between zero and some fixed amplitude. An example of this type of disturbance is grinding, where the force is always in one direction, for example the positive x-direction, and varies with the rotational speed of the tool, and so has a constant, known frequency content. Figure 5 shows a block diagram representation of how APACA fits into the total system with the non-adaptive lead-filter compensators.

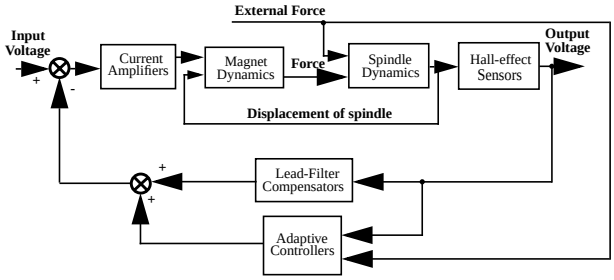

Figure 5. Block diagram including adaptive controller

APACA calculates successive estimates of the amplitude and phase of a complimentary input sine wave that will combine with the disturbance to create zero net motion. The signal from the adaptive controller must go through the amplifier and magnet dynamics before driving the spindle motion through the bearing magnets. Therefore even if the exact disturbance time history is known, it cannot simply be inverted and used directly to cancel itself out. Also, in grinding applications, the amplitude of the disturbance may not be known, but the frequency most likely will be. If the frequency is not known, it can be determined by using an FFT (fast Fourier transform) algorithm on the output signal to determine the dominant frequencies, and then those frequencies can be used in APACA.

Two parameters are varied in determining the output of APACA; the amplitude of the wave A and the phase shift from the disturbance wave (actually computed as a time delay T where $\phi = \omega T$). The output then looks like

$$y_A = A(\sin(\omega t + \omega T) + 1) \tag{18}$$

where ω is the frequency of the disturbance and is assumed to be known.

The two variable parameters are calculated according to a modified MIT Rule. The sensitivity derivative is replaced by the time derivative of the error signal in the time delay equation and by a constant in the amplitude equation (which is absorbed by the constant γ_A). The error signal in the time delay equation is replaced by the disturbance signal. These modifications lead to the recursive equations which form the basis of APACA,

$$A(n+1) = A(n) + \gamma_A e(n) \tag{19}$$

$$T(n+1) = T(n) + \gamma_T \frac{de(n)}{dt} d(n) \tag{20}$$

SIMULATION AND HARWARE

These equations were implemented in Simulink using the parameters shown in Table 3.

Table 3: Simulation parameters

parameter	value
γ_A	1×10^{-5}
γ_T	1×10^{-9}
sample time	0.1 ms

These parameters were found through testing the controller in simulation and on the experimental setup and trying to find a balance between short convergence time and stability. Like the MIT Rule, a poor selection for γ_A and γ_T (a value that is too large) may result in system instability. However, values that are too small will result in long convergence times and a system that won't be able to adapt to changing disturbances.

RESULTS

The system was tested in simulation with a disturbance input of 0.5 N and frequency of 100 Hz. On the hardware, this corresponded to an input current of 2.3 amps. The results are shown in the following figures. In order to increase the stability of the system, APACA is not implemented in the simulation until after the transient rigid body motion has been damped out by the onboard analog controllers. The time at which APACA is turned on is marked on the plots. The maximum range of the spindle motion is $\pm40\times10^{-5}$ m, but normal operating range is $\pm15\times10^{-5}$ m, so the displacement of the spindle shown in Figure 6 and Figure 7 is near the limit of the normal operating range. There was a small amount of noise injected into the current amplifier signal in the simulation in order to determine its effects on the adaptation algorithm. The power of this noise was determined from steady-state experimental data.

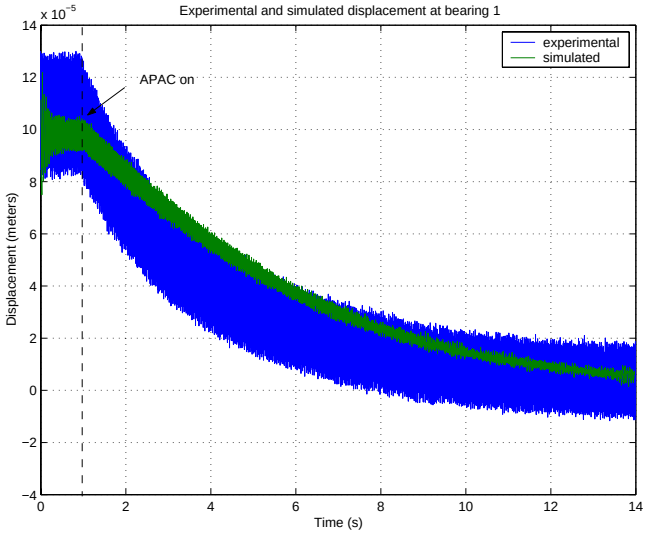

Figure 6. Graph of x1 displacement with controller on

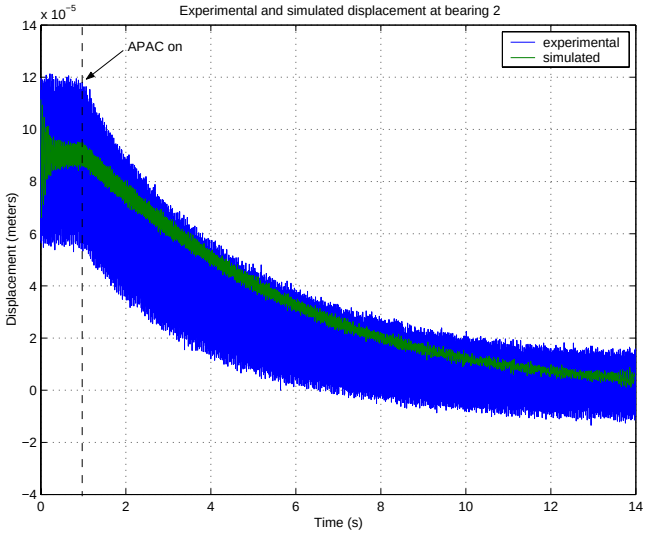

Figure 7. Graph of x2 displacement with controller on

Figure 6 shows the simulated displacement of the spindle at bearing 1 in the x-direction and Figure 7 shows the displacement at bearing 2. (Since the external force is not applied at the center of the spindle, the results at bearing 1 and bearing 2 are not identical.) For $0 \le t < 1$ s, the external force is applied with just the analog lead-filter compensators in place. This results in oscillation about a value offset from zero. At $t = 1$ s, APACA is turned on and begins to add its signal to the system input. The displacement is quickly reduced and the spindle reaches its equilibrium position approximately 2 seconds after the controller is implemented.

In the simulation, APACA attenuated the amplitude of oscillation at bearing 1 and bearing 2 by -10.5 dB and -8.5 dB respctively. On the hardware, the oscillation was decreased by -5.3 dB at bearing 1 and -7.6 dB at bearing 2. These results are summarized in Table 4.

Table 4: Experimental and simulated attenuations of oscillation amplitude

	Simulated	Experimental
bearing 1	-10.5 dB	-5.3 dB
bearing 2	-8.5 dB	-7.6 dB

The output signal of APACA is shown in Figure 8. In the simulation, the final values to which A and T converge are 0.286 V and 3.3×10^{-4} s respectively. This corresponds to an amplitude of 0.25 N and a phase shift of 0.033 rad, or $1.9°$. Since there are two bearings acting to counteract the external force, we would expect each to exert a force with an amplitude of half of the external force. The phase shift is due to the dynamics of the magnets and amplifiers.

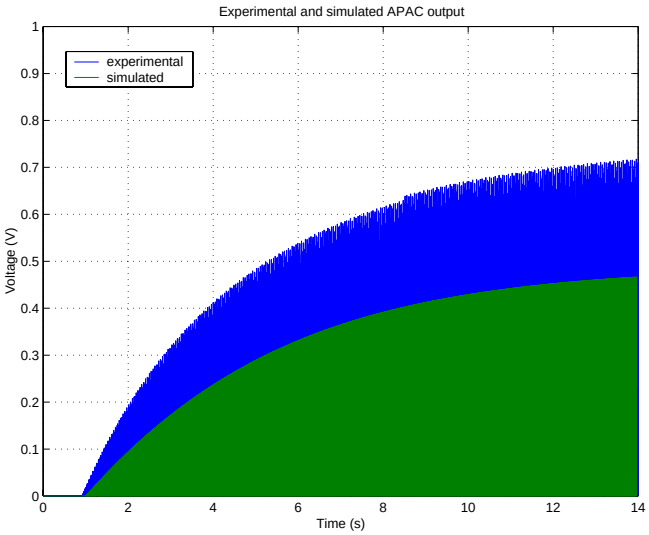

Figure 8. APACA output for experimental and simulation

Due to the complexity and uncertainties of the bearing system, the experimental results did not match with the simulated results as closely as expected. Fortunately, this data provides an opportunity to increase the accuracy of the simulation for future control algorithm design and testing

CONCLUSION AND FUTURE WORK

The two parameter adaptive control algorithm presented here yielded considerable reduction in steady-state displacement in both simulation and experiment for an externally applied sinusoidal load. Future enhancements to the current design will include four parameters to adjust in the output; the amplitude of the sine wave, the frequency of the sine wave, the phase shift, and the offset from zero. These enhancements will allow the algorithm to handle a constant disturbance, a sine wave oscillating about zero, or a sine wave of unknown or slowly varying frequency.

Ultimately, this type of algorithm will applied to a magnetic bearing grinder. A picture of a grinder rotor/bearing system is shown in Figure 9. This system is currently installed in a test stand so that system identification and control algorithm testing can begin with an actual grinding system.This algorithm could help reduce unwanted motion of the spindle which leads to poor part finish and chatter.

Figure 9. Magnetic rotor/bearing system for grinder

REFERENCES

Paden, B., “Operating Manual for the MBC500,” Magnetic Moments, Inc., Santa Barbara CA.

Isermann, R. et al., Adaptive Control Systems, Prentice Hall, 1992.

Barney, P. et al., “Adaptive spindle balancing using magnetically levitated bearings”, Proceedings of the 1999 IMECE.

Distribution

MS 0557	Thomas J. Baca (09125)
MS 0501	Patrick S. Barney (02338) (5 copies)
MS 0841	Tomas C. Bickel (09100)
MS 0509	Michael W. Callahan (02300)
MS 0960	Norman E. Demeza (14100)
MS 9405	Michal T. Dyer (08700)
MS 0555	Mark S. Garrett (09122)
MS 9042	James L. Handrock (08727)
MS 0501	Ming K. Lau(2338)
MS 9042	James P. Lauffer (08727) (5 copies)
MS 0847	David M. Martinez (09124)
MS0847	Rodney A. May (09126)
MS0188	Charles E. Meyers (01030)
MS 0847	Harold S. Morgan (09123)
MS 0958	Alan R. Parker (14184)
MS 0847	James M. Redmond (09124) (5 copies)
MS 0958	William N. Sullivan (14184) (5 copies)
MS 0899	Tech Library (09616) (2 copies)
MS 0612	Review and Approval Desk (9612) for DOE/OSTI (1 copies)
MS 9018	Central Technical Files (8945-1)

Prof. Brad Paden
Magnetic Moments, Inc
5735 Hollister Avenue, Suite B
Goleta, CA 93117
Santa Barbara, CA

Prof. Gordon Parker
Michigan Technical University
1400 Townsend Dr.
Houghton, MI 49931
(5 copies)